All-Fiber Curvature Sensor Based on an Abrupt Tapered Fiber and a Fabry–Pérot Interferometer

Martin Cano-Contreras, Ana D. Guzman-Chavez, Ruth I. Mata-Chavez, Everardo Vargas-Rodriguez, Daniel Jauregui-Vazquez, David Claudio-Gonzalez, Julian M. Estudillo-Ayala, Roberto Rojas-Laguna, and Eduardo Huerta-Mascotte

***Abstract*— In this letter, a highly sensitive curvature sensor arrangement based on an abrupt tapered fiber (ATF) concatenated with an all-fiber micro Fabry–Pérot interferometer (MFPI) is presented. Here, as the ATF is bent, the MFPI spectral fringes contrast decreases. In addition, the curvature sensitivity is considerably enhanced due to the use of the ATF. Finally, it is shown that with this arrangement, at 1530-nm wavelength, it is possible to detect curvature changes with a sensitivity of 11.27 dB/m^{-1} and a curvature resolution of 8.87×10^{-3} m^{-1} within the measurement range of $0 - 3.5$ m^{-1}.**

***Index Terms*— Optical fiber sensors, Fabry–Pérot interferometer, tapered fiber, curvature.**

I. Introduction

SINCE long time ago, fiber optic sensors have been widely studied due to their multiple applications and features such as compactness, low cost, immunity to electromagnetic interference and high sensitiveness. Particularly, all-fiber optic curvature sensors have won special interest because of their flexibility to be used in different potential applications, for instance in robot arms and monitoring structural deformations of buildings [1]. Therefore, multiple fiber optic arrangements for bend sensing can be found in literature, which are based on different optical devices, as for instance: long period fiber gratings (LPG) written in D-shaped optical fibers [2], a pair of LPG [3], LPG inscribed in holey fibers [4], and hybrid LPG with a tilted fiber Bragg grating [5], etc. Furthermore, optical curvature sensors based on modal interferometers have been also reported. Some of these arrangements are based on uniform fiber Bragg gratings [6], [7], tapered photonic crystal fiber [8] and two concatenated tapers to enhance the sensor sensitivity [9]. Moreover some designs based on microcavity Fabry–Pérot interferometers, fabricated within micro structured holey fibers, have been proposed [10]. In general, interferometric optical sensors are widely used since these have excellent optical properties [11]–[13] and additionally because of these are relatively easy to manufacture and fairly inexpensive since usually only a fusion splicer is required for their implementation.

In this letter we present a highly sensitive curvature sensing scheme based on an abrupt tapered fiber concatenated with a micro Fabry–Pérot interferometer (MFPI). This MFPI is implemented in a hollow core photonic crystal fiber (HCPCF). Here, the interferometer's cavity is an air microbubble which was fabricated by applying electric discharges to the HCPCF with a conventional fusion splicer. Afterwards, this MFPI was concatenated with an ATF in order to modify the modal field diameter (MFD), which enhances the curvature sensitivity. In this way the MFPI fringes contrast decreases as the ATF is bent. This allowed our sensing arrangement to detect curvature changes with high sensitivity. Finally some experimental results and conclusions are provided.

II. Fabrication of the Sensing Element

The sensing element used in this letter was based on a MFPI concatenated with an ATF. The fabrication process of the MFPI was described in detail by [14]. In figure 1 steps of the procedure followed to fabricate the sensing element are shown. Basically, this procedure involves the next steps: 1) A micro structured fiber segment (HC-1064-19 Cells Fiber Crystal) and a single mode fiber (SMF), are cleaved at right angle and afterwards are placed on a conventional splicer (Fitel-S175) at the reference position (the electrodes get positioned between the two fibers) (Fig. 1-a); 2) Both fibers are displaced a distance D = 80 μm from the reference position, at this stage the splicer electrodes get over the SMF (Fig. 1-b); 3) Both fibers are coupled and spliced without collapsing the HCPCF holes; 4) The spliced fibers are displaced a distance L in backward direction, here the electrodes get over the HCPCF (Fig. 1-c); 5) The HCPCF gets broken by applying multiple electric discharges and finally an air MFPI is obtained at the tip of the SMF (Fig. 1-d). Moreover, the obtained MFPI (Fig. 2-a) has a thin silica wall of thickness l (Fig. 1-d). It is important to mention that the displacements D and L were performed by using the manual mode of the fusion splicer and after each one of the applied electric discharges

Manuscript received July 15, 2014; accepted August 6, 2014. Date of publication August 26, 2014; date of current version October 20, 2014. This work was supported in part by the SEP-PROMEP under Project UGTO-PTC-341, in part by the Universidad de Guanajuato, under Project 088/2012, in part by the National Council of Science and Technology (CONACYT)-Gobierno del Estado de Guanajuato under Project GTO-2012-C04-193904, and in part by the CONACYT under Project 166361.

M. Cano-Contreras, A. D. Guzman-Chavez, R. I. Mata-Chavez, E. Vargas-Rodriguez, D. Claudio-Gonzalez, and E. Huerta-Mascotte are with the Division de Ingenierias Campus Irapuato-Salamanca, Departamento de Estudios Multidisciplinarios, Universidad de Guanajuato, León 37000, Mexico (e-mail: mcano_cco@utsoe.edu.mx; ad.guzman@ugto.mx; ruth@ugto.mx; evr@ugto.mx; dclaudio@ugto.mx; ehuerta@utsoe.edu.mx).

D. Jauregui-Vazquez, J. M. Estudillo-Ayala, and R. Rojas-Laguna are with the Division de Ingenierias Campus Irapuato-Salamanca, Departamento de Electronica, Universidad de Guanajuato, León 37000, Mexico (e-mail: jaureguid@ugto.mx; julian@ugto.mx; rlaguna@ugto.mx).

Color versions of one or more of the figures in this letter are available online at http://ieeexplore.ieee.org.

Digital Object Identifier 10.1109/LPT.2014.2349979

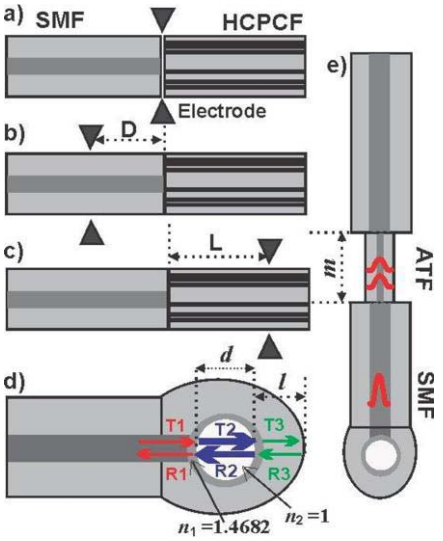

Fig. 1. a) - c) Steps of the MFPI fabrication process, d) reflections involved in the MFPI, and e) diagram of the MFD modified at the ATF.

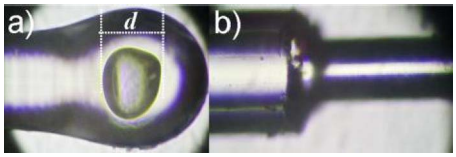

Fig. 2. Pictures of a) the MFPI and b) the ATF.

the alignment process was not used. Finally, to obtain our sensing element, at the other end of the SMF with the MFPI, the segment with the ATF was spliced (Fig. 1-e). The taper was based on standard fiber (SMF-28) and it was fabricated by using a Vytran glass processor system. The ATF (Fig. 2-b) used in this letter had a diameter of 60 μm and a length of 2.8 cm. Here it is important to mention that the ATF bending sensitivity increases as its diameter gets narrowed. Therefore for characterization purposes we tried with different ATFs and it was observed that for narrow diameters these were very fragile and often easily get broken when curvature was applied. In our case ATFs with diameters over the 60 μm were more resistant and supported without problem the mechanical stress induced by bending. For this reason, we decided to use an unpacked ATF with 60 μm which was sufficiently resistant for our sensor characterization purposes. Here, in order to protect the ATF the curvature was applied over the flexible iron sheet (Fig. 3).

III. Experimental Setup

The experimental setup used to carry out the curvature measurements is shown in figure 3. Here, the light of a pigtailed diode laser, emitting at $\lambda = 980$ nm and delivering a maximum output power of 200 mW, was coupled to a wavelength division multiplexer (Qphotonics QFBGLD-980-200) to pump an erbium doped fiber (Newport F-EDF-T3) of 3.4 m length. Afterwards, the luminescence generated by the EDF travels towards the sensing device (ATF-SMF-MFPI) through the circulator (Thorlabs 6015-3), from the port 1 to the port 2. Finally, the reflected interference spectrum of the MFPI was monitored at the port 3 of the circulator by using an optical spectrum analyzer (OSA, Yokogawa AQ6370C), which was set with a resolution of 0.02 nm.

Here, the tapered fiber segment was fixed to a flexible iron sheet, which was suspended over two lateral slots. The distance between the two slots is $2S = 9$ cm. The ATF's center was positioned just in the middle of the metallic sheet. At this point, but in the other side of the iron sheet, a micrometer screw was also positioned in order to induce a fiber bending (see inset of Fig. 3). In this arrangement the curvature can be easily calculated by using the formula:

$$C = \frac{1}{R} = \frac{2h}{h^2 + S^2} \tag{1}$$

where R is the curvature radius and h is the vertical displacement measured from the center of the metallic sheet without curvature. Moreover, it is important to mention that due to the flexibility of the iron sheet and the system design the bending was induced in a descending form in order to obtain curvature measurements with high precision.

A. Operating Principle of the Sensing Device

The principle of operation of our sensing device is explained by means of the interference phenomenon occurring within the MFPI and by the ATF losses due to macro bending effects. The interference spectrum of the MFPI used in this letter is ideally formed by the interference of three reflections, which are generated at the three interfaces of the MFPI (Fig. 1-d). The first reflection (R1) occurs at the interface formed by the silica of the SMF core and the air (Figure 1-d), here the silica has a refractive index $n_1 = 1.4682$. Afterwards the transmitted light (T1) travels through the main MFPI cavity, which is an air microcavity with length d and $n_2 = 1$. Here the second reflection (R2) is generated. Finally, the transmitted light beam (T2) propagates a distance l through the third and last interface, which is formed by the silica and the medium around the tip of the MFPI, where the third reflection (R3) occurs. In this case the silica refractive index is considered as $n_1 = 1.4682$ and as the surrounding medium of the MFPI is air, therefore $n_3 = 1$. In this way, ideally the MFPI spectrum will be formed mainly by two superimposed Fabry–Pérot interferometer (FPI) spectra, one is generated within the main FPI cavity and the second one within the thin silica wall at the tip. However, the air cavity and the silica wall characteristics will depend on some fabrication parameters such as the distance L and the number of arc discharges [14]. Therefore, by varying these parameters it is possible to attenuate the FPI spectrum occurring at the silica wall, allowing the interference pattern occurring at the micro air cavity govern the overall FPI spectrum. Hence, in the inset of figure 4, the measured transmittance pattern of our MFPI is shown, where it can be observed that it has only one well defined FPI spectrum with a $\Delta\lambda = 8.1$ nm. For a single cavity FPI the separation between two consecutive spectral fringes it is known as the free spectral range ($\Delta\lambda$) and it can be calculated by using the formula [15]:

$$\Delta\lambda = \frac{\lambda^2}{2nd} \tag{2}$$

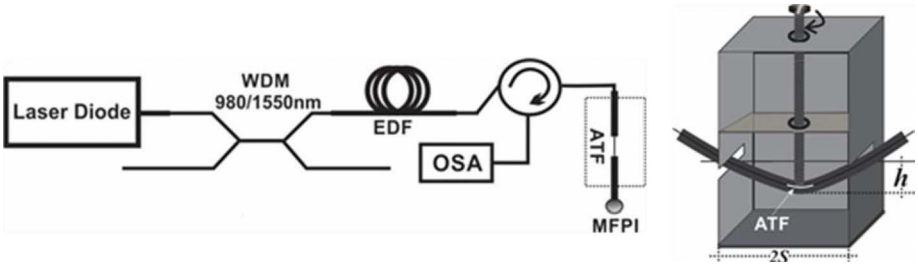

Fig. 3. Experimental diagram of the sensing scheme for curvature measurements.

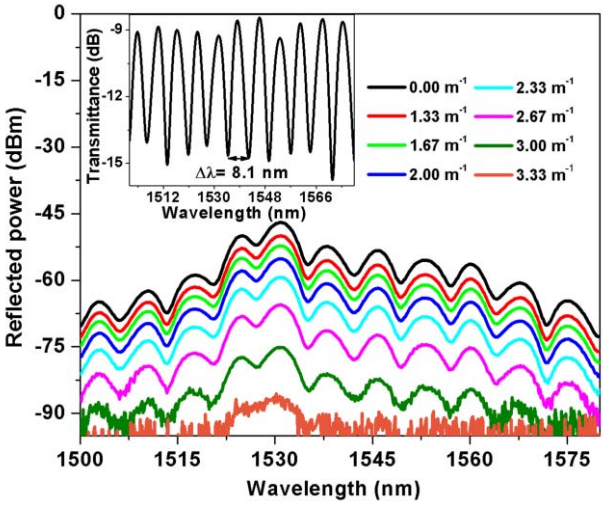

Fig. 4. Measured MFPI spectra for different curvature values. Inset: measured transmittance spectrum for C = 0 m^{-1}.

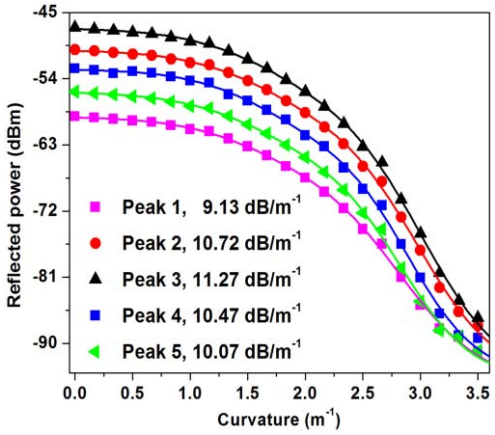

Fig. 5. Measurement of the reflected power for different MFPI spectral fringes as a function of the curvature.

where λ is the reference wavelength and nd is the optical thickness of the FPI cavity, being for our case $n = 1$. Therefore by using (2) it is possible to determine that the length of the microcavity was around $d = 144$ μm (Fig. 2-a).

Now, the reflected interference spectrum of the MFPI will pass through the ATF. Here, let us to recall that when a fiber optic is bent, with a certain curvature radius, losses in the guided light transmission will occur [16] since the field distribution is modified. Consequently, in the fiber segment where bending is applied some light travelling by the core will leak to the cladding, reducing the light confined within the core. Additionally, the curvature sensitivity can be enhanced by increasing the MFD (Fig. 1-e), which can be done by changing the contrast between the core and the cladding refractive indexes Δn_e [17]. For instance, in a tapered fiber the core diameter is reduced significantly and therefore Δn_e became almost zero. Consequently, the guiding in this tapered fiber segment is governed by the interface cladding-air (Fig. 1-e), which presents a high Δn_e and therefore the field distribution covers a significant portion of the cladding [18], [19]. Therefore, small curvature changes in the ATF will induce significant losses in the reflected interference pattern of the MFPI.

IV. Experimental Results

Reflected spectra for different curvature values and generated using a pump power of 105.6 mW are shown in figure 4. Here it can be observed that as the curvature increases, the reflected power is attenuated. This is because of the macro bending effects occurring inside the ATF, as was previously mentioned.

As can be seen in figure 4, the curvature sensitivity of each spectral fringe directly depends on the shape of the luminescence spectrum of erbium [20]. For example, we analyzed the behavior of the fringes 1, 2, 3, 4, and 5 which peaks are centered at wavelengths of 1517.4, 1524.9, 1530.8, 1538.0 y 1553.1 nm respectively (Fig. 4). The reflected power of each fringe as a function of the curvature is presented in figure 5. Here it can be observed that exists a strong relationship between the intensity of the FPI fringes and the curvature. In our case, for the fringe 3, the maximum curvature sensitivity achieved was 11.27 dB/ m^{-1} within the curvature range from 0 to 3.5 m^{-1}. In a previous work, we reported a curvature sensor where the ATF was not used [10]. In that work we achieved a maximum curvature sensitivity of 0.3 dB/m^{-1} and a curvature range from 40 – 100 m^{-1}. Comparing these values, it can be appreciated how the ATF helps to enhance the overall sensor performance.

Moreover, by considering that the OSA used to perform the experiments has an amplitude resolution of 0.1 dB, it is possible to state that the curvature resolution for this arrangement is in the order of 8.87×10^{-3} m^{-1}. Furthermore to ensure the repeatability of our sensing device, different curvature measurements tests were performed (Fig. 6), which shown a standard deviation of ± 0.23 dB. This implies that our sensor

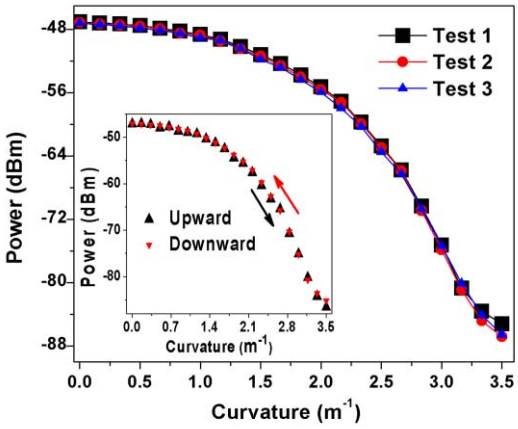

Fig. 6. Measured reflected power of the peak 1 as a function of the curvature for different tests. Inset: measured reflected power of the peak 1 as a function of the curvature applied in upward and downward direction.

device has excellent repeatability. It is important to point out that the curvature measurements in downward direction presents a standard deviation of ± 0.18 dB with respect to the first test carried out in upward direction, which means that the sensor device has a low hysteresis (inset of Fig. 6).

Finally, it is important to mention that drifting errors can affect the sensor response. The drift can be induced by changes in the power source, in the temperature of the sensing element and by aging of the components. In our case the effects due to temperature of the sensing element can be considered as negligible since the thermo optic coefficient of silica is very small ($+0.5 \times 10^{-6}\ {}^{0}\mathrm{C}^{-1}$) [21]. However, the sensor can be more sensitive to drifting errors due to power source variations and therefore if necessary an additional compensation stage must be used. In literature different compensation setups can be found, as for instance the cross correlation systems, which are based on two optical channels, one for reference and one for measurement [22], [23]. A similar stage can be relatively simple added to our sensing setup, however by the moment we focused in the characterization of the overall sensing arrangement which is based on the ATF-FPI structure.

V. Conclusions

In this letter a highly sensitive curvature sensing arrangement based on an abrupt tapered fiber concatenated with a hollow core photonic crystal fiber micro Fabry–Pérot interferometer was demonstrated. In this arrangement, the reflected power of the interference pattern, generated by the MFPI, is modified by the curvature changes applied to the ATF. Here the abrupt taper was used to enhance the sensor sensitivity taking advantage of the increment of the mode field diameter in the cladding zone. Thus, the sensitivity and the resolution of our sensing arrangement were 11.27 dB/m^{-1} and 8.87×10^{-3} m^{-1} respectively, within the curvature range from 0 to 3.5 m^{-1}. Our sensing arrangement showed an excellent repeatability and presented a practically negligible hysteresis. Finally it is important to point out that the sensing arrangement can be enhanced by adding a compensation system to reduce drifting errors.

References

[1] H. J. Patrick, C. C. Chang, and S. T. Vohra, "Long period fibre gratings for structural bend sensing," *Electron. Lett.*, vol. 34, no. 18, pp. 1773–1775, Jul. 1998.
[2] T. Allsop, A. Gillooly, V. Mezentsev, T. Earthgrowl-Gould, R. Neal, D. J. Webb, and I. Bennion, "Bending and orientational characteristics of long period gratings written in D-shaped optical fiber [directional bend sensors]," *IEEE Trans. Instrum. Meas.*, vol. 53, no. 1, pp. 130–135, Feb. 2004.
[3] Y. G. Han, B. H. Lee, W.-T. Han, U.-C. Paek, and Y. Chung, "Fibre-optic sensing applications of a pair of long-period fibre gratings," *Meas. Sci. Technol.*, vol. 12, no. 7, pp. 778–781, 2001.
[4] Y. G. Han, G. Kim, K. Lee, S. B. Lee, C. H. Jeong, C. H. Oh, and H. J. Kang, "Bending sensitivity of long-period fiber gratings inscribed in holey fibers depending on an axial rotation angle," *Opt. Exp.*, vol. 15, no. 20, pp. 12866–12871, Oct. 2007.
[5] L.-Y. Shao, A. Laronche, M. Smietana, P. Mikulic, W. J. Bock, and J. Albert, "Highly sensitive bend sensor with hybrid long-period and tilted fiber Bragg grating," *Opt. Commun.*, vol. 283, no. 13, pp. 2690–2694, 2010.
[6] W. Zhou, Y. Zhou, X. Dong, L.-Y. Shao, J. Cheng, and J. Albert, "Fiber-optic curvature sensor based on cladding-mode Bragg grating excited by fiber multimode interferometer," *IEEE Photon. J.*, vol. 4, no. 3, pp. 1051–1057, Jun. 2012.
[7] X. Dong *et al.*, "In-line fiber Mach–Zehnder interferometer combining with fiber Bragg grating for simultaneous curvature and temperature measurement," *Proc. SPIE*, vol. 8199, pp. 819903–819908, Nov. 2011.
[8] K. Ni, T. Li, L. Hu, W. Qian, Q. Zhang, and S. Jin, "Temperature-independent curvature sensor based on tapered photonic crystal fiber interferometer," *Opt. Commun.*, vol. 285, pp. 5148–5150, Aug. 2012.
[9] D. Monzon-Hernandez, A. Martinez-Rios, I. Torres-Gomez, and G. Salceda-Delgado, "Compact optical fiber curvature sensor based on concatenating two tapers," *Opt. Lett.*, vol. 36, no. 22, pp. 4380–4382, Nov. 2011.
[10] D. Jauregui-Vazquez, J. M. Estudillo-Ayala, A. Castillo-Guzman, R. Rojas-Laguna, R. Selvas-Aguilar, E. Vargas-Rodriguez, J. M. Sierra-Hernandez, V. Guzman-Ramos, and A. Flores-Balderas, "Highly sensitive curvature and displacement sensing setup based on an all fiber micro Fabry–Perot interferometer," *Opt. Commun.*, vol. 308, pp. 289–292, Jul. 2013.
[11] S. J. Petuchowski, T. G. Giallorenzi, and S. K. Sheem, "A sensitive fiber-optic Fabry–Perot interferometer," *IEEE J. Quantum Electron.*, vol. 17, no. 11, pp. 2168–2170, Nov. 1981.
[12] G. E. Town, K. Sugden, J. A. R. Williams, I. Bennion, and S. B. Poole, "Wide-band Fabry–Perot-like filters in optical fiber," *IEEE Photon. Technol. Lett.*, vol. 7, no. 1, pp. 78–80, Jan. 1995.
[13] J. Ma, J. Ju, L. Jin, and W. Jin, "A compact fiber-tip micro-cavity sensor for high-pressure measurement," *IEEE Photon. Technol. Lett.*, vol. 23, no. 21, pp. 1561–1563, Nov. 1, 2011.
[14] D. Jauregui-Vazquez, J. M. Estudillo-Ayala, R. Rojas-Laguna, E. Vargas-Rodriguez, J. M. Sierra-Hernandez, J. C. Hernandez-Garcia, and R. I. Mata-Chavez, "All fiber intrinsic Fabry–Perot interferometer based on an air-microcavity," *Sensors*, vol. 13, no. 5, pp. 6355–6364, May 2013.
[15] E. Hecht, *Fabry–Perot Spectroscopy in Optics*, 4th ed. Upper Saddle River, NJ, USA: Pearson, 2002, pp. 412–425.
[16] D. Marcuse, "Curvature loss formula for optical fibers," *J. Opt. Soc. Amer. B*, vol. 66, no. 3, pp. 216–220, Mar. 1976.
[17] A. Mendez and T. F. Morse, *Methods to Improve Performance in Specialty Optical Fibers Handbook*, 1st ed. San Francisco, CA, USA: Academic, 2007, pp. 227–232.
[18] A. Hartung, F. Wirth, and H. Bartelk, "Light propagation in tapered optical fibers: Spatial light confinement and generation of plasmonic waves," in *Proc. PIERS*, Mar. 2011, pp. 255–258.
[19] L. C. Bobb, P. M. Shankar, and H. D. Hrumboltz, "Bending effects in biconically tapered single-mode fibers," *J. Lightw. Technol.*, vol. 8, no. 7, pp. 1084–1090, Jul. 1990.
[20] M. J. F. Digonnet, *Rare Earth Doped Fiber Lasers and Amplifiers*, 2nd ed. New York, NY, USA: Marcel Dekker, 1993, pp. 29–33.
[21] T. Zhu, D. Wu, M. Liu, and D.-W. Duan, "In-line fiber optic interferometric sensors in single-mode fibers," *Sensors*, vol. 12, no. 8, pp. 10430–10449, Aug. 2012.
[22] A. Wang, H. Xiao, J. Wang, Z. Wang, W. Zhao, and R. G. May, "Self-calibrated interferometric-intensity-based optical fiber sensors," *J. Lightw. Technol.*, vol. 19, no. 10, pp. 1495–1501, Oct. 2001.
[23] P. Chambers, E. A. D. Austin, and J. P. Dakin, "Theoretical analysis of a methane gas detection system, using the complementary source modulation method of correlation spectroscopy," *Meas. Sci. Technol.*, vol. 15, no. 8, p. 1629, 2004.